Mechanism of electron-spin resonance studied with use of scanning tunneling microscopy

D. Shachal and Y. Manassen
Department of Chemical Physics, The Weizmann Institute of Science, Rehovot 76100, Israel
(Received 15 April 1992)

The observation of the precession frequencies of individual paramagnetic spins with use of scanning tunneling microscopy is explained here by a spin-orbit-coupling mechanism. Excitation of the paramagnetic dangling bond into a superposition of states will lead to charge-density oscillations, which add a time-dependent term to the tunneling barrier. The nonlinear dependence of the tunneling current on the barrier shape will give rise to a Larmor frequency component in the tunneling current. It is shown how the signal should be affected by different parameters, such as the relative orientations between the tunneling electrons and the dangling bond or the initial spin excitation. Possibilities that will be opened with this technique, as well as the questions that will have to be resolved, are discussed.

I. INTRODUCTION

The field of surface science has experienced a revolution in the past ten years with the invention of the scanning tunneling microscope (STM).[1,2] The STM is capable of imaging conducting surfaces, either semiconductors[2] or metals.[3] It was found to be very useful in exploring a wide variety of systems. Examples are determination of the surface structure,[2] observation of vacancies and steps,[4,5] determination of the structure of molecules adsorbed on surfaces,[6] observation of local changes in both geometric and electronic structure as a result of a chemical reaction,[7] study of nucleation and growth processes,[8] and real-time imagine of dynamical processes such as migration of steps.[9] While most of the STM experiments are carried out under UHV (ultrahigh vacuum) conditions, atomic resolution was observed also in air[10] and under various liquids.[11] The technique was successfully operated in a wide temperature range: from liquid-helium temperature[12] to 900 °C.

While most of the earlier studies have concentrated on topographic imaging of surfaces, it was realized later that the STM can be very useful in studying local physical phenomena. Such physical phenomena can either be used as a local probe to control the position of the tip (instead of the tunneling current) or can be measured simultaneously with it. Examples are photon emission,[13] potentiometry,[14] conductivity,[15] atomic forces,[16] capacitance,[17] and temperature.[18] An example which is relevant to this publication is the observation of the precession frequencies of individual paramagnetic spins—with the STM.[19]

Because of its local character, the STM should be sensitive to any local perturbation which is close enough to the tunneling region to affect the tunneling probability. As will be explained here, such a perturbation could be caused by an electron spin at a surface, when an external static magnetic field is present. Our work showed that indeed a paramagnetic spin is capable of modulating the tunneling current by inducing a time-dependent periodic perturbation on the tunneling electrons, resulting in a local rf signal at the Larmor frequency, when the tunneling region was close to the spin center. The magnetic field was chosen to be small enough such that the observed signals were still in the rf regime. The rf signal was amplified by a rf amplifier and was detected at a frequency which is (within experimental error) the Larmor frequency. The frequency was proportional to the magnetic field and the observed signals were correlated with a lateral position of the tip above the surface and were restricted to regions of approximately 15 Å in diameter. A similar rf signal was observed also in our laboratory in Israel in preliminary measurements on the same system.

Recently, rf tunneling current was observed from spin centers which are large free radical molecules. [α,γ-bis(diphenylene)-β-phenylally (BDPA)].[20] The rf current intensity observed in this experiment was much weaker than in the first one. As a result, magnetic-field modulations and lock-in detection techniques were employed in order to make the rf signal detectable.

The first experiment was carried out on a SI(111)7×7 surface which was thermally oxidizing. Such a treatment gives a Si-SiO_2 interface which has a large number of spin centers. These spin centers are present (in smaller numbers) in the Si-SiO_2 interface of native silicon oxide layers, and give rise to several localized states within the silicon band gap. These interface states are a source of many problems in the metal-oxide-semiconductor (MOS) technology. One of the most important spin centers in this group is the P_b center, which was investigated by conventional ESR spectroscopy.[21] The first ESR-STM experiment was done on these spin centers, since they show a detectable ESR signal at room temperature and since silicon surfaces are convenient to study with the STM.

According to macroscopic ESR studies, the P_b spin center exhibits C_{3v} symmetry, where the symmetry axis is perpendicular to the (111) Si-SiO_2 interface.[22] Using very sensitive ESR techniques, it was possible to observe the hyperfine spectrum associated with spin centers in which the central silicon atom was a low natural abundant ^{29}Si isotope. The size of the hyperfine coupling constant indicated that 80% of the unpaired spin density is localized on the central-trivalent bonded silicon atom, and that the hybrid orbital on this silicon atom is 12% *s*-like and 88%

$p(111)$-like.[23] As a result it was concluded that the spin center is a trivalent silicon atom located at the Si-SiO_2 interface and that the unpaired electrons are localized in a $|SP^3\rangle$-like hybrid orbitals (Fig. 1)

II. MODEL OF THE SPIN CENTER

In modeling the spin center we make the crude approximation of looking at a defect "molecule" and ignoring the overlap with the bulk solid. We start by writing the Hamiltonian of the system: electronic plus spin and diagonalizing it. The model spin center is an isolated silicon atom in the Si-SiO_2 interface. In a bulk silicon crystal the symmetry of the atom is tetrahedral. As a result the eigenfunctions which describe the system are the four hybridized $|SP^3\rangle$ orbitals that will be denoted by $|SP_i^3\rangle$, $i=0,1,2,3$. The coordinate system is chosen such that the $|SP_0^3\rangle$ orbitals is in the [111] direction. In these orbitals seven electrons are filled. The singly occupied orbital of the spin center is higher in energy than the doubly occupied orbitals pointing to the bulk. The energy difference is Δ. The ground-state configuration of the radical "molecule" is such that one electron is in the $|SP_0^3\rangle$ orbital and six in the others. This state is doubly degenerate (Kramers degeneracy). The excited-state configuration will be sixfold degenerate (Fig. 2). This system is entirely equivalent to having one electron in the $|SP_0^3\rangle$ orbital. Therefore a single-electron problem can be solved.

The tetrahedral symmetry of the spin center is broken; therefore, a more accurate treatment of the orbital eigenfunctions has to take into consideration some mixing between the $|SP^3\rangle$ orbitals. The result will be that the orbital of the paramagnetic electron will have a larger $|P_z\rangle$ component. This is supported, as was mentioned before, by ESR spectroscopy. This correction, however, will not change the basic predictions of the model and will not be included.

Since the system can be treated as a single-electron problem, the functions $|SP_0^3\alpha\rangle, |SP_0^3\beta\rangle, \ldots, |SP_3^3\beta\rangle$ are chosen as a basis for the Hamiltonian. Without any mixing interactions these are the eigenfunctions of the system. This is no longer the case after the spin-orbit coupling introduces off-diagonal elements between these states. The matrix elements of the Hamiltonian were calculated by applying the operator $\xi\mathbf{L}\cdot\mathbf{S}$ on the $|SP^3\rangle$ orbitals[24] (Appendix A). ξ is the spin-orbit coupling constant. $\mathbf{L}$ and $\mathbf{S}$ are the orbital and the spin angular momenta. The spin-orbit coupling splits the sixfold degenerate level into threefold degenerate levels with splittings given by δ_i, $i=1,2,3$ giving four doubly degenerate Kramers doublets (Fig. 2).

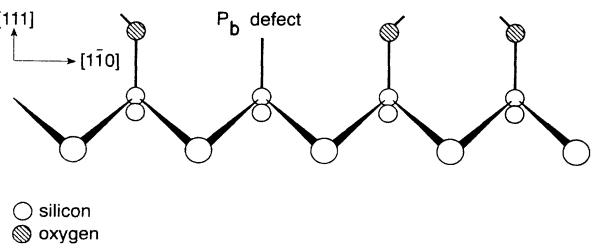

FIG. 1. The P_b center—the unpaired electron is localized in a dangling hybrid bond on a silicon atom which is covalently bonded to the three lower silicon atoms. This center exists where an oxygen atom is not bonded to the surface crystalline silicon atom.

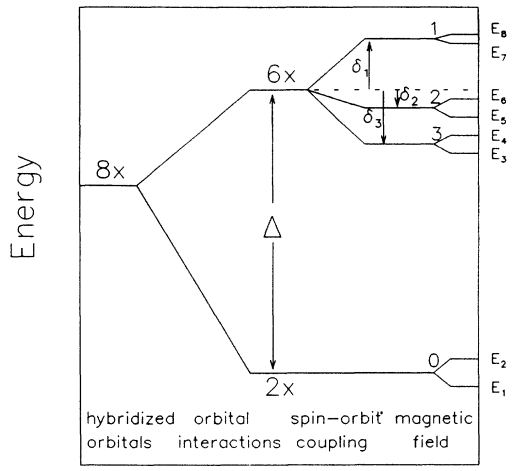

FIG. 2. A scheme of the electronic energy levels as split by the molecular interactions (Δ), the spin-orbit coupling, and the magnetic field.

Applying an external magnetic field will add an additional term to the Hamiltonian. This Zeeman term will act as a small perturbation which will remove the degeneracy between all the Kramers doublets. The matrix elements of the Zeeman term $\mathcal{H}_{\text{Zeeman}}=\mu_B(\mathbf{L}+g_e\mathbf{S})\cdot\mathbf{H}$ (μ_B is the Bohr magneton and $\mathbf{H}$ is the magnetic field) in the basis $|SP_0^3\alpha\rangle, \ldots, |SP_3^3\beta\rangle$ were calculated (Appendix A).

The Zeeman splittings which were introduced by the magnetic field will be denoted by $g_0\mu_B H$, $g_1\mu_B H$, $g_2\mu_B H$, and $g_3\mu_B H$ (Fig. 2). $g_0\mu_B H$ is the ground-state Zeeman transition which is normally observed with ESR spectroscopy.

In order to calculate the eigenenergies of this system, perturbation theory can be applied. The advantage of the perturbative solution is that analytical expressions can be developed and give a better physical insight to the result. Here, the perturbation treatment can be applied twice: first, since $\xi \ll \Delta$ and second since $g\mu_B H \ll \xi$ (Appendix B). In addition, numerical diagonalization of the Hamiltonian gives a more accurate (but numerical) solution. The elements of this Hamiltonian are given in Appendix A. The numerical solution is used in the calculations which are reported here.

The splittings of the ground-state Zeeman transition (E_2-E_1) is found as expected to be dependent on the orientation of the magnetic field. The perturbative solution shows that when the magnetic field is parallel to the dangling bond $(H_x=H_y=H_z=H/\sqrt{3})$, $g=g_e$. When the field is parallel to the x, y, or z axes, $g=g_e+\xi/\Delta$. When the field is parallel to the other $|SP_3\rangle$ orbitals, $g_0=g_e+4\xi/3\Delta$. As usual, the anisotropy of the g tensor reflects the symmetry of the spin center. Since the size of the g anisotropy can be estimated from experimental

measurements of the ESR spectra, ξ/Δ could be evaluated to be 0.01.[21]

The splittings of the excited Kramers doublets (E_4-E_3, E_6-E_5, and E_8-E_7) are much more anisotropic than the ground-state one. This is a manifestation of the interplay between the spin-orbit coupling and the electrostatic or chemical interactions which causes the removal of the degeneracy (Δ). Removal of the degeneracy between states which have the same quantum number of the orbital angular momentum results in quenching of the orbital angular momentum. The spin-orbit coupling restores some of the quenched momentum. The fraction of the restored orbital angular momentum will be ξ/Δ. As a result the ground-state Zeeman transition has a small anisotropic contribution of the orbital angular momentum. The Zeeman transitions in the excited electronic states ($g_1\mu_B H$, $g_2\mu_B H$, and $g_3\mu_B H$) are possessing full orbital angular momentum (and large anisotropy), since no electrostatic or chemical interaction (at least we assume so in this simplified model) is removing the sixfold degeneracy of the excited states.

III. TIME EVOLUTION OF THE SPIN CENTER

As known from inelastic tunneling spectroscopy, the tunneling electrons are capable of exciting different modes in tunneling junctions. This is true in particular in the STM since the tunneling electrons are restricted to a very small region. The problem of the excitation is a very complicated one and was not completed yet. It is clear, however, that the excitation is quite significant. Such an excitation will lead to a superposition of eigenstates, namely to a time-dependent behavior. The charge density in the $|SP_0^3\rangle$ orbitals will become time dependent. In order to show that indeed such a time evolution should lead to a modulation of the tunneling current at the precession frequencies, this time evolution, as given by the Schrödinger equation, will be calculated. Any excitation of the spin center will drive it into a superposition of eigenstates

$$|\Psi(t_0)\rangle=\sum_i b_i|u_i\rangle \quad \text{where } b_i=\langle u_i|\Psi(t_0)\rangle \ .$$

This state will evolve according to the Schrödinger equation

$$|\Psi(t)\rangle=\sum_i b_i \exp\left[\frac{-iE_i(t-t_0)}{\hbar}\right]|u_i\rangle \ .$$

The most important interaction between the tunneling electrons and the spin center is Coulombic interaction. Exchange and correlation interactions are expected to play a significant role at closer distances. We will initially consider the case where the tunneling is performed directly above the spin center. In this case the Coulombic interactions are not capable of breaking the symmetry of the spin center. Such an interaction can only reduce the size of Δ. Therefore, the excited state $|\Psi(t_0)\rangle$ was calculated by taking a smaller value of Δ in the original Hamiltonian. Then the Hamiltonian was diagonalized and a set of eigenvectors $|v_i\rangle$ were calculated. It should be emphasized that the eigenvectors $|v_i\rangle$ are not eigenvectors of the original unperturbed Hamiltonian (labeled $|u_i\rangle$), but are superpositions of them.

As will be shown later, the strongest time-dependent signal is observed when the system is initially excited into a superposition of spin states. Therefore the initial state is taken as a superposition in which the two ground spin states of the perturbed Hamiltonian (labeled $|v_i\rangle$) and $|v_2\rangle$) are taken with equal weights, namely we start with a complete spin superposition

$$|\Psi(t_0)\rangle=\frac{1}{\sqrt{2}}(|v_1\rangle+|v_2\rangle) \ .$$

As the perturbation is removed, the dynamics is calculated with the help of the eigenvectors $|u_i\rangle$ and the eigenvalues E_i of the unperturbed Hamiltonian. The time evolution of the charge density in the $|SP_0^3\rangle$ orbitals $\rho_{|SP_0^3\rangle}(t)$ is calculated. The excitation will lead to a time-dependent charge density which is a sum of several oscillating components. The frequencies correspond to the energy differences between the eigenstates.

Rearranging the expression for this sum of complex exponential functions results in a sum of slowly modulated oscillating functions,

$$\rho_{|SP_0^3\rangle}(t)=a_0+\sum_n a_n \sin(\omega_n t)\sin(\Omega_n t) \ .$$

a_0 is the time-independent "static" part of $\rho_{|SP_0^3\rangle}(t)$, a_n is the intensity of the nth oscillatory component. The size of the different a_n is dependent first of all on the spin-orbit coupling. When this will vanish, no modulated functions will appear. The spin-orbit coupling provides the upper limit for the different a_n. The observation of a weaker signal of BDPA (Ref. 20) relative to the P_b center is consistent with the smaller spin-orbit coupling of carbon as compared with silicon. The actual size of these a_n is dependent on the process of excitation. It is important to emphasize—and it will be shown—that such a time evolution of $\rho_{|SP_0^3\rangle}(t)$ is observed after any excitation. For example, it is observed even if it does not take place exactly above the spin center or if the initial state is in a pure spin state (namely the initial state is either $|v_1\rangle$ or $|v_2\rangle$).

$\rho_{|SP_0^3\rangle}(t)$ appears to be a sum of several "beat" functions. Relevant to our case are components in which the beat is a product of a "fast" oscillating function at a frequency ω_n corresponding to $(\Delta+\delta_i)/\hbar$ ("electronic" frequencies) and a "slow" oscillating function at a frequency Ω_n corresponding to one-half of the Zeeman transition ($g_0\mu_B/H/2\hbar$). The frequencies Ω_n and ω_n are a result of interference between two functions oscillating at the frequencies $(E_{ex}-E_1)/\hbar$ and $(E_{ex}-E_2)/\hbar$, where E_1 and E_2 are the two ground-state Zeeman energy levels and E_{ex} is an excited electronic energy level. Each excited state should contribute one beat function with $\Omega_n=(g_0\mu_B H)/2\hbar$. There should be six such functions. Due to symmetry considerations only four have a nonzero amplitude.

Figure 3 shows the intensity of one of the four components, which has $\Omega_n=g_0\mu_B H/2\hbar$, as a function of the

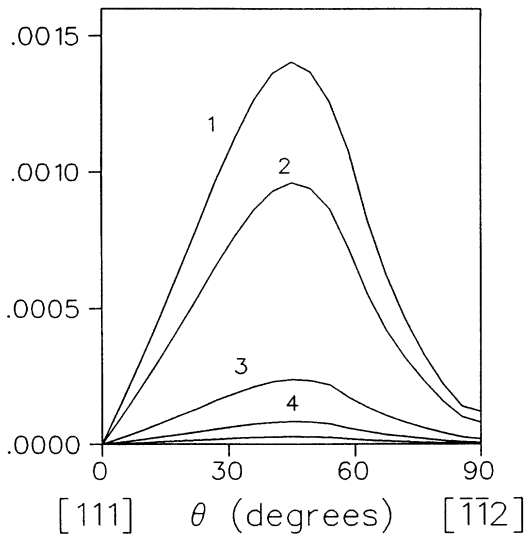

FIG. 3. The amplitudes of one term (out of four) contributing to the Zeeman frequency signal as a function of the intensity of the excitation. This excitation intensity is changed in the calculation by changing the value of ξ/Δ in $(|v_1\rangle+|v_2\rangle)/\sqrt{2}$: $\xi/\Delta=1$ (curve 1), $\xi/\Delta=0.5$ (curve 2), $\xi/\Delta=0.1$ (curve 3), $\xi/\Delta=0.04$ (curve 4), and $\xi/\Delta=0.01$ (lower curve).

size of electrostatic perturbations [by changing the size of Δ in $(|v_1\rangle+|v_2\rangle)/\sqrt{2}$] and as a function of the direction of the magnetic field. When the magnetic field is parallel to the $|SP_0^3\rangle$ orbital, and no symmetry breaking is introduced, the amplitude is zero. This can be associated with the absence of precessing orbital angular momentum when the field is in this direction ($g_0=g_e$ in conventional ESR spectroscopy in this case). The other three components have a similar but not identical behavior.

The case discussed above, in which the tunneling occurs directly above the spin center, is a very special case. It is more realistic to assume that the electrostatic interactions will break the symmetry of the spin center. Figure 4 shows that when this is the case, a small deviation from symmetric excitation gives a significantly different and larger oscillatory component. Our calculations indicate that a nonsymmetric perturbation can create a more pronounced excitation than a symmetric one. In this case, the amplitude will be nonzero, even if the magnetic field is parallel to the dangling bond.

An additional important question is whether the system has to be with an initial spin superposition in order to give a nonzero oscillatory function with $\Omega_n=g_0\mu_B H/2\hbar$ (i.e., whether a superposition of $|v_1\rangle$ and $|v_2\rangle$ is required). At the moment we assume that the system is present initially in this superposition of spin states. Nevertheless, excitation into a superposition of spin states by the tunneling electrons is a possibility which must also be taken into account. Our calculations show that the size of the initial spin superposition has a very important effect. In the case of a weak electrostatic perturbation, if the initial state is not spin polarized [$|\Psi(t_0)\rangle=|v_1\rangle$, for example] than the intensity of the calculated oscillating component is zero. When a stronger electrostatic perturbation is applied on the system this is no longer the case, but still, even in such cases, the initial spin superposition has a significant affect on the intensity of the calculated oscillating components (Fig. 5).

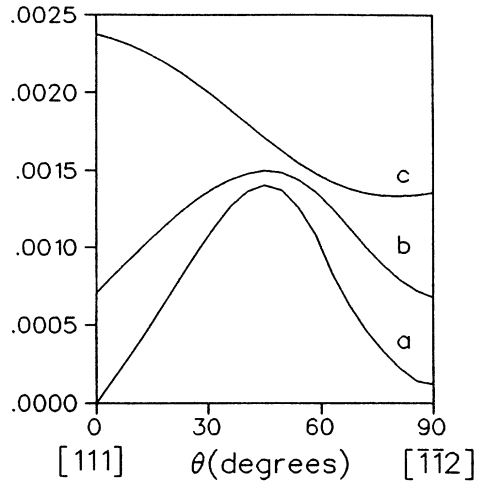

FIG. 4. The amplitudes of the Zeeman term (same as in Fig. 3) when the excitation is not "symmetric." Curve *a* is the same as curve 1 in Fig. 3 ("symmetric" excitation). In curve *b*, in addition to taking $\xi/\Delta=1$, the energy of levels 7 and 8 is lifted by $\xi/4$ in the excited state. In curve *c* the energy is lifted by ξ.

To summarize, any excitation will drive the system into a superposition of states. This leads to a time evolution which is modulated by the Larmor frequency. In the following it will be shown how the nonlinear characteristics of the STM leads to a direct observation of the Larmor frequency.

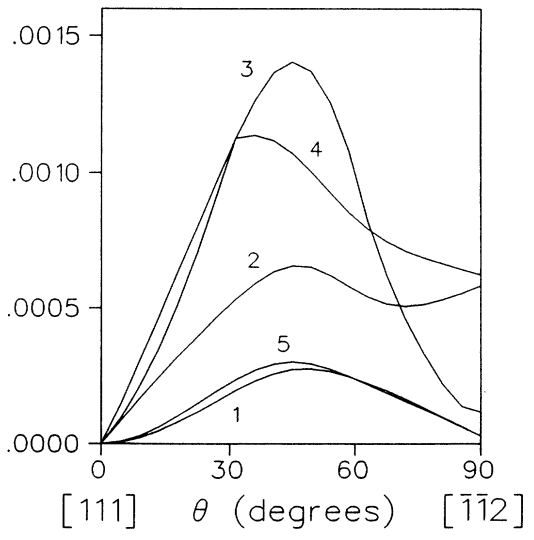

FIG. 5. The amplitudes of one term (out of four) contributing to the Zeeman frequency signal as a function of the size of the initial spin superposition. The amplitudes are shown for different coefficients of the initial state $c_1|v_1\rangle+c_2|v_2\rangle$: $c_1=1$ (curve 1), $c_1=3c_2$ (curve 2) $c_1=c_2$ (curve 3), $c_2=3c_1$ (curve 4), and $c_2=1$ (curve 5).

IV. OBSERVATION OF A LARMOR FREQUENCY COMPONENT AT THE TUNNELING CURRENT

As was shown above, any excitation is capable of leading to time-dependent charge-density oscillations in the paramagnetic dangling bond. In a close proximity to the spin center, the tunneling process will be affected by these oscillations. This can be attributed to several mechanisms. First, the Coulombic interaction between the oscillating charge density and the tunneling electrons will add a time-dependent term to the static potential energy $V_0(x)$ as represented by the barrier shape:

$$V(x,t)=V_0(x)+\sum_n V_n \sin(\omega_n t)\sin(\Omega_n T) .$$

Second, the tunneling current is sensitive also to the barrier width. The charge-density oscillations affect the barrier width by changing the classically forbidden region. Barrier width oscillations were used, for example, in the detection of surface acoustic waves with the STM.[25] In addition, these oscillations are expected to affect the local density of states—at the Fermi level. The tunneling current in a planar tunnel barrier can be expressed as $J(t)\alpha\exp\{-A[V(x,t)]^{1/2}d\}$, where $A=[8\pi m_e/\hbar]^{1/2}$, $V(x,t)$ is the barrier height, and d is the barrier width. Due to the exponential dependence of the tunneling current on the barrier height and width, the gap exhibits nonlinear behavior. If $J(t)$ was a linear function of $V(x,t)$, than only components with frequencies $\omega_i+\Omega_i$ and $\omega_i-\Omega_i$ will be observed in $J(t)$ [i.e., only the frequency components of $V(x,t)$ itself]. As a result of the nonlinear dependence of $J(t)$ on $V(x,t)$, the sum and difference frequencies, $2\Omega_n$, $2\omega_n$, and 0 will be observed as well. This nonlinear dependence gives rise to the observation of the Larmor frequency of individual paramagnetic spins. The ability to observe sum and difference frequencies was exploited in STM detection of surface acoustic waves.[25] In our case, four components of $\rho_{|SP_0^3\rangle}(t)$ have oscillating terms with the frequency difference $2\Omega_n=\omega_L$ (the Larmor frequency). The intensity of this ω_L component which was measured experimentally depends on the degree of the nonlinearity of the STM. This can be easily understood by looking at the series expansion of the exponential function: $e^{-x}=1-x+x^2/2!-x^3/3!+\cdots$. As $x\to 0$, the nonlinear character of the gap becomes rather small. For increasing x, it is expected that the nonlinearity of the STM, as well as the amplitude of the Larmor frequency component, will be bigger.

An order of magnitude calculation can be performed in order to estimate the contribution of the barrier height modulations to the Larmor frequency component of the tunneling current. Considering only Coulombic interactions, the potential can be estimated by ee_d/r, where e_d is the charge in the dangling bond and r is the distance between it and the tunneling electron. By taking this form of interaction we ignore the electrostatic interaction with the static nuclear charge. We are only interested here in the time-dependent term in the potential due to the charge-density oscillations. The relevant time-dependent term in the charge density is

$$e_d(t)=\eta e \sin(\Omega_n t)\sin(\omega_n t) ,$$

where η is the ratio between the oscillating charge density and the constant charge density. Assuming $\eta=0.01$ (considering the contribution of all four relevant components and ignoring the difference in the frequency of the "fast" components—$\omega_n s$), the contribution of the oscillating barrier amounts to several tens of meV for $d=4$–8 Å. The intensity of the difference frequency component $J(2\Omega_n=\omega_L)$ can be calculated by a numerical Fourier transform of $J(t)$.

In Figure 6 the amplitude of the original $(\Omega_n+\omega_n)$ and the difference $(2\Omega_n)$ frequencies as a function of the ratio a/b is shown for different tunneling distances, where a is the static potential and b is the time-dependent potential. As can be seen, the relative intensity of the difference frequency component increases with the gap distance, a fact which is consistent with a larger nonlinear response of the STM at larger distances.

In the experimental system, the design of the rf requipment was such that a detection limit of 10^{-10} A rf current was assumed. The actual sensitivity was better and the detection limit was in the order of magnitude of 10^{-11} A rf current. Even with a tunneling current of several nanoamperes (this was indeed the case in most of the experiments), especially for cases of smaller tunneling distances, the ratio a/b cannot be more than 5 in order to pass the detection limit of the Larmor frequency component. This implies a very small static barrier ($\sim$0.2 eV). The barrier height at large tip-sample distances is an average between the work functions of the tip and the sample, which amounts to several electron volts in our case. However, as the barrier width is reduced, the barrier height is becoming smaller according to the simplified formula $V=V_\infty-\alpha/d$, where V_∞ is the barrier height at infinity (average of work functions), d is the barrier width, and $\alpha\sim 10$ eV Å. (This formula is true only for $d>2$ Å, where the reduction[26] in V is mainly due to image forces.) Although barrier heights of the order of 0.2 eV can be observed according to this formula it

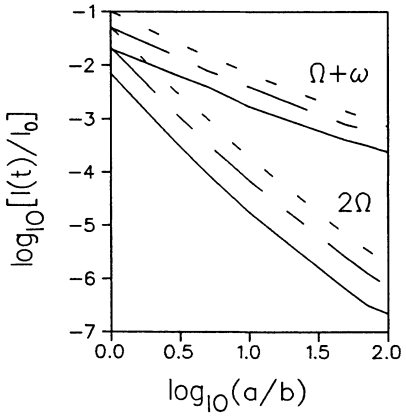

FIG. 6. The amplitudes of the principle frequency $(\Omega+\omega)$ and the difference frequency (2Ω) as a function of the ratio between the constant and the modulated barrier height (a/b) for a gap distance of 4 Å (solid curve), 6 Å (dashed curve), and 8 Å (dotted curve). The amplitudes are calculated relative to the dc tunneling current.

seems that this value (of the static barrier height) is somewhat unrealistic. This discrepency can be resolved in several ways: First, only the impact of the charge-density oscillations on the barrier height was considered, ignoring a similar impact on the barrier width. Including the impact of the barrier width modulations will increase the ω_L component, resulting in a detectable signal for much larger barrier heights.

In addition, in this treatment we ignored the nonlinearity of the STM which is a result of the nonuniform density of states on the semiconductor surface. This gives rise to a nonlinear response in the IV curve. Including this nonlinearity in the STM response to the charge-density oscillations will increase the amplitude of the ω_L component.

In our model a value of $\eta=0.01$ was taken. This is based on the value of ξ/Δ observed from ESR spectroscopy. However, this value was observed for a "free" spin center (namely, a spin center on which no chemical or electrostatic interactions are applied). The strong interactions induced by the tip may reduce the size of Δ in the spin center. Such interactions have attracted significant attention recently, since they play a role in many STM phenomena. The reduction in Δ will increase the size of the oscillating components relative to the static one leading to a much larger value of η. Our calculations indicate that for $\eta=0.1$ the oscillating components should be detectable for barrier heights of several electron volts. Although the problem of the amplitude of the ω_L oscillating component has to be further elaborated, it was shown above that such a component does exist. We showed that the nonlinear dependence of J on V plays a crucial role in this effect. This point was not well elaborated in a previous paper.[27]

V. DISCUSSION

The Larmor frequency component can be detected when an excitation is driving the paramagnetic dangling bond into a superposition of states. Despite the fact that the excitation is primarily electrostatic, the spin-orbit coupling introduces modulations at the Larmor frequency into the time evolution. The excitation is probably a result of several competing processes. It is an extremely complicated problem. Although such a calculation has not been completed yet, we are able to draw at this stage several qualitative conclusions.

The tunneling electrons interact with the spin center through Coulombic, exchange, and correlation interactions. As the electron tunnels through the junction it may transfer a fraction of its energy to any elementary excitation to which it may couple. It is well established that tunneling electrons may excite vibrational modes of adsorbed molecules in tunneling junctions.[28] There are several experimental evidences of exciting electronic transitions in organic molecules[29] and rare-earth oxides[30] using inelastic tunneling spectroscopy. Using STM for exciting optical transitions in the visible range,[31] photon emission was observed. In these processes parity conservation rules are slightly lifted.[32] This is attributed to the mixing of functions with different parity by the strong electric field in the barrier. Direct Coulombic interactions between the tunneling electrons and the dangling bond are most probably the main cause of excitation.

The tunneling electrons may also excite phonons in tunneling junctions.[28] These lattice vibrations create time-dependent modulations of the local electric field. These modulations, although weaker than those which are a result of the direct electrostatic interactions with the tunneling electrons, are still capable of creating a pronounced excitation—leading to a superposition of states. An additional possible source of excitation is via modulation of the spin-orbit coupling. It should be recalled that the spin-orbit coupling is proportional to (and is a result of) the electric field applied by the screened charge of the nucleus on the electron. It is quite clear that the strength of the electric field applied on the spin center by the tunneling electrons (and to a lesser extent by the biased tip) is approaching the order of magnitude of the nuclear charge field. It is therefore expected that a continuous change in the size of the spin-orbit coupling might also play a role in the excitation process.

A problem which must be taken into account is the dephasing associated with the excitation process. If each electron will destroy the phase of the superposition, the signal will not be detectable. In cases where the electrostatic perturbation is not too strong, the spin polarization is only weakly and indirectly affected by it—via the spin-orbit coupling, and therefore the Larmor frequency modulation will continue from the point where it was before the perturbation. (This is similar to the requirement for an initial spin superposition for having a nonzero amplitude modulation—as was discussed above.) This is no longer true when the electrostatic perturbations are strong. In this case it is quite clear that the spin polarization will also be affected.

The change of the modulation as a result of the (strong) electrostatic perturbation should be slowly varying on a time scale of the Larmor precession in order to prevent a complete dephasing of the signal. The time scale of a single tunneling process is of the order of femtoseconds. A typical tunneling current in the STM is $J\sim 10^{-9}$ A, implying 10^{10} electrons per second. Therefore each such process could be treated independently. In a Larmor frequency of 10^9 Hz, if the probability of excitation will be 1 or even 0.1, no signal will be observed. An order of magnitude calculation for the probability of excitation of vibrational modes of an adsorbed CO molecule gives an excitation probability of 0.01.[33] A more precise answer to the problem associated with the interplay between excitation and dephasing will have to be answered by a more detailed model. This problem can be addressed experimentally by changing the magnitude of the magnetic field. In the limit of slow precession, many tunneling electrons will interact with the precessing spin during one cycle and will dephase the signal. In the high-field limit the regular relaxation processes will dominate.

The theory must be further developed in order to provide more quantitative answers to many problems, some of which were mentioned above. There are many questions which have to be addressed experimentally in order

to test the theoratical predictions. Examples of such further research directions are as follows.

(1) The theory predicts that the frequency of modulation will be the Larmor frequency of the ground-state Zeeman transition (as measured with conventional ESR spectroscopy). This means a dependence of the frequency on the direction of the magnetic field (g anisotropy). Although it will be quite difficult to determine the direction of the magnetic field relative to the individual spin center on the microscopic level, an attempt will be made to follow the dependence of the frequency of the signal on the direction of the magnetic field.

(2) The question whether spectroscopic information can be observed with this technique is of course of central importance. For example, ESR spectroscopy is used in order to determine the symmetry of the spin center through, for example, the anisotropy of the g tensor. (In the spin center discussed here, this is a C_{3v} symmetry.) However, the spin center under the STM tip probably has different properties than the "free" spin center measured under normal conditions in ESR. Unfortunately, it is possible that the information regarding the symmetry of the spin center will be completely destroyed by the strong and partially random electric field applied by the tip, which is only a factor of 10 or so smaller than the field applied on the electrons by the nucleus. (Since the forces applied by the tunneling electrons are so instantaneous they are not expected to change this information, i.e., to change the eigenvalues and eigenvectors of the spin center.) The chemical interactions between the tip and the spin center might also have a similar effect. These questions will be addressed experimentally.

(3) Regarding the observation of spectroscopic information, the question of observing a hyperfine spectrum is of great interest. The appearance of such a spectrum will be entirely different than in the macroscopic hyperfine spectrum which is an ensemble average. Looking at one spin, it is expected that only one line of the hyperfine spectrum will be observed (corresponding to a certain orientation of the interacting nuclei). After some time the signal will jump to a different frequency. The time between the jumps is expected to be related to the spin-lattice relaxation of the interacting nuclei.

(4) An extremely important question will be how the lifetimes of all the states will affect the signal. It is conjectured that the signal should be dependent more on the different relaxation times of the different ESR transitions, and less on the different electronic lifetimes. The arguments are similar to those in the case of the interplay between excitation and dephasing; electronic excitation processes are not expected to affect significantly the ESR transitions. (It does so only indirectly through the spin-orbit coupling.) Predicting the precise affect of the relaxation processes requires a more detailed treatment of the problem. These predictions can be compared with experiments on different spin centers, for example, by saturating the ground-state Zeeman transition with an external strong rf field. Creating an initial spin superposition with an external rf field should affect the intensity of the signal as was discussed earlier. Working at different temperatures might also provide useful information regarding these processes.

From studies by the ESR spectroscopy, 80% of the unpaired electron density is localized on the central Si atom of the defect, while 98% of it is located on the $Si(Si)_4$ cluster which consists of the central Si atom and the four atoms bound to it. It is an important question: What will be the predictions of the model when the molecular orbitals of the extended system [the $Si(Si)_4$ cluster] are taken into account. In this way several conclusions about the role of localization might be obtained. This question is extremely important, since it is intended to study spin centers on conducting surfaces. Of similar interest is the question of the optimal size of the spin-orbit coupling. A large spin-orbit coupling, while leading to a larger signal, will probably lead to relaxation processes which are too rapid, leading (at room temperature) to a complete broadening of the signal. This question may be tested by performing the experiment on different spin centers.

Recently an alternative theory on this effect was developed.[34] According to this theory, the Larmor frequency component is explained by a singularity in the tunneling current, which arises due to coherent tunneling of pairs of electrons with opposite spins accompanied by a spin reversal of both electrons in the course of this scattering of the paramagnetic center. Several experimental tests must be done in order to check the predictions of both theories and the validity of each model.

According to the model which is discussed in our paper, the spin-orbit coupling of the examined spin center is the only reason for observing the Larmor frequency component. The alternative theory gives this role to the spin-orbit coupling of the atom at the apex of the tip. Replacing the tip material, so that the tip atoms will have a different atomic number, will help to elucidate which model provides the correct prediction.

While the reason for changes in the signal intensity are numerous and complicated, as has been discussed in detail in this paper, the alternative model predicts a much simpler relation for the intensity ratio between the Larmor frequency components (JJ_ω) and the static component of the tunneling current (J_0). This intensity ratio is (using the terminology of this paper[34])

$$\frac{d\ln|JJ_\omega|}{dz}\Big/\frac{d\ln|J_0|}{dz}=2\ ,$$

where z here is the gap width. This relation can be directly tested by changing the size of the dc tunneling current.

In summary, the ESR-STM experiments raise many questions which have to be resolved. Further developments in this research direction will provide STM the capability to follow many interesting fundamental phenomena and to obtain chemical information on individual surface spin centers.

ACKNOWLEDGMENTS

The authors would like to express their deep gratitude to Professor Shimon Vega for many useful discussions. This work was done under a partial support of the U.S.–Israel Binational Science Foundation and the Basic Research Foundation administered by the Israeli Academy of Science.

APPENDIX A

1. The matrix elements of $\xi \mathbf{L}\cdot\mathbf{S}$ (including Δ)

We have

	$\lvert SP_0^3\alpha\rangle$	$\lvert SP_0^3\beta\rangle$	$\lvert SP_1^3\alpha\rangle$	$\lvert SP_1^3\beta\rangle$	$\lvert SP_2^3\alpha\rangle$	$\lvert SP_2^3\beta\rangle$	$\lvert SP_3^3\alpha\rangle$	$\lvert SP_3^3\beta\rangle$
$\langle \alpha SP_0^3\rvert$	Δ	0	0	$\frac{\xi}{4}-i\frac{\xi}{4}$	$-i\frac{\xi}{4}$	$i\frac{\xi}{4}$	$i\frac{\xi}{4}$	$-\frac{\xi}{4}$
$\langle \beta SP_0^3\rvert$	0	Δ	$-\frac{\xi}{4}-i\frac{\xi}{4}$	0	$i\frac{\xi}{4}$	$i\frac{\xi}{4}$	$\frac{\xi}{4}$	$-i\frac{\xi}{4}$
$\langle \alpha SP_1^3\rvert$	0	$-\frac{\xi}{4}+i\frac{\xi}{4}$	0	0	$i\frac{\xi}{4}$	$\frac{\xi}{4}$	$-i\frac{\xi}{4}$	$-i\frac{\xi}{4}$
$\langle \beta SP_1^3\rvert$	$\frac{\xi}{4}+i\frac{\xi}{4}$	0	0	0	$-\frac{\xi}{4}$	$-i\frac{\xi}{4}$	$-i\frac{\xi}{4}$	$i\frac{\xi}{4}$
$\langle \alpha SP_2^3\rvert$	$i\frac{\xi}{4}$	$-i\frac{\xi}{4}$	$-i\frac{\xi}{4}$	$-\frac{\xi}{4}$	0	0	0	$\frac{\xi}{4}+i\frac{\xi}{4}$
$\langle \beta SP_2^3\rvert$	$-i\frac{\xi}{4}$	$-i\frac{\xi}{4}$	$\frac{\xi}{4}$	$i\frac{\xi}{4}$	0	0	$-\frac{\xi}{4}+i\frac{\xi}{4}$	0
$\langle \alpha SP_3^3\rvert$	$-i\frac{\xi}{4}$	$\frac{\xi}{4}$	$i\frac{\xi}{4}$	$i\frac{\xi}{4}$	0	$-\frac{\xi}{4}-i\frac{\xi}{4}$	0	0
$\langle \beta SP_3^3\rvert$	$-\frac{\xi}{4}$	$i\frac{\xi}{4}$	$i\frac{\xi}{4}$	$-i\frac{\xi}{4}$	$\frac{\xi}{4}-i\frac{\xi}{4}$	0	0	0

2. The matrix elements of $\mu_B(g_e\mathbf{S}+\mathbf{L})\cdot\mathbf{H}$

We have the expression as given on the following page.

APPENDIX B

The first step in x the perturbative treatment is applying $\xi\mathbf{L}\cdot\mathbf{S}$ as a perturbation to the unperturbed Hamiltonian, where $\langle \alpha SP_0^3|\mathcal{H}_0|SP_0^3\alpha\rangle = \langle \beta SP_0^3|\mathcal{H}_0|SP_0^3\beta\rangle = \Delta$ and the other elements are zero. First-order nondegenerate perturbation theory can be applied in order to find the corrected eigenfunctions $|SP_0^3\alpha\rangle_1$ and $|SP_0^3\beta\rangle_1$, provided that $\xi \ll \Delta$,

$$|SP_0^3\alpha\rangle_1 = |SP_0^3\alpha\rangle_0 + \sum_i \frac{\langle \Psi_i|\xi\mathbf{L}\cdot\mathbf{S}|SP_0^3\alpha\rangle}{E_0-E_i}|\Psi_i\rangle ,$$

where $|\Psi_i\rangle$ is the ith eigenfunction which is mixed by the perturbation with $|SP_0^3\alpha\rangle_0$ and E_0-E_i is the energy difference between them. The same expression holds for $|SP_0^3\beta\rangle_1$. The eigenfunctions $|SP_1^3\alpha\rangle$, $|SP_1^3\beta\rangle, \ldots, |SP_3^3\beta\rangle$ are mixed as a result of the perturbation. These states are originally degenerate. The removal of the degeneracy is calculated with the help of degenerate perturbation theory. Since all elements in the 6×6 matrix spanned by the six degenerate functions $|SP_1^3\alpha\rangle$, $|SP_1^3\beta\rangle, \ldots, |SP_3^3\beta\rangle$ contain the element ξ (Appendix *A* 1), this matrix can be numerically diagonalized. If the coupling of the functions $|SP_1^3\alpha\rangle, \ldots, |SP_3^3\beta\rangle$ with $|SP_0^3\alpha\rangle$ and $|SP_0^3\beta\rangle$ is ignored, then numerical diagonalization of the Hamiltonian, giving us the six linear combinations $|\Psi_3\rangle, \ldots, |\Psi_8\rangle$ of the basis functions $|SP_1^3\alpha\rangle, \ldots, |SP_3^3\beta\rangle$ is completing the diagonalization to first order in $\xi\mathbf{L}\cdot\mathbf{S}$.

The energies of the resulted states $|SP_0^3\alpha\rangle_1$, $|SP_0^3\beta\rangle_1$, $|\Psi_3\rangle, \ldots, |\Psi_8\rangle$ form a set of four Kramers doublets. Their degeneracy can be removed by an external magnetic field. The Zeeman term causes mixing between the doubly degenerate states. Thus we have to diagonalize four 2×2 matrices which are created by applying this term on the four pairs of degenerate eigenvectors. Since the Zeeman term was applied as a second, smaller perturbation (namely, $g\mu_B H \ll \xi$) it was possible to ignore all the other coupling terms.

	$\lvert SP_0^3\alpha\rangle$	$\lvert SP_0^3\beta\rangle$	$\lvert SP_1^3\alpha\rangle$	$\lvert SP_1^3\beta\rangle$	$\lvert SP_2^3\alpha\rangle$	$\lvert SP_2^3\beta\rangle$	$\lvert SP_3^3\alpha\rangle$	$\lvert SP_3^3\beta\rangle$
$\langle \alpha SP_0^3 \rvert$	$\frac{\mu_B g_e H_z}{2}$	$\frac{\mu_B g_e (H_x - iH_y)}{2}$	$\frac{-i\mu_B H_x + i\mu_B H_y}{2}$	0	$\frac{i\mu_B H_x - i\mu_B H_z}{2}$	0	$\frac{-i\mu_B H_y + i\mu_B H_z}{2}$	0
$\langle \beta SP_0^3 \rvert$	$\frac{\mu_B g_e (H_x + iH_y)}{2}$	$\frac{-\mu_B g_e H_z}{2}$	0	$\frac{-i\mu_B H_x + i\mu_B H_y}{2}$	0	$\frac{i\mu_B H_x - i\mu_B H_z}{2}$	0	$\frac{-i\mu_B H_y + i\mu_B H_z}{2}$
$\langle \alpha SP_1^3 \rvert$	$\frac{i\mu_B H_x - i\mu_B H_y}{2}$	0	$\frac{\mu_B g_e H_z}{2}$	$\frac{\mu_B g_e (H_x - iH_y)}{2}$	$\frac{i\mu_B H_y + i\mu_B H_z}{2}$	0	$\frac{-i\mu_B H_x + i\mu_B H_z}{2}$	0
$\langle \beta SP_1^3 \rvert$	0	$\frac{i\mu_B H_x - i\mu_B H_y}{2}$	$\frac{\mu_B g_e (H_x + iH_y)}{2}$	$\frac{-\mu_B g_e H_z}{2}$	0	$\frac{i\mu_B H_y + i\mu_B H_z}{2}$	0	$\frac{-i\mu_B H_x + i\mu_B H_z}{2}$
$\langle \alpha SP_2^3 \rvert$	$\frac{-i\mu_B H_x + i\mu_B H_z}{2}$	0	$\frac{-i\mu_B H_y - i\mu_B H_z}{2}$	0	$\frac{\mu_B g_e H_z}{2}$	$\frac{\mu_B g_e (H_x - iH_y)}{2}$	$\frac{i\mu_B H_x + i\mu_B H_y}{2}$	0
$\langle \beta SP_2^3 \rvert$	0	$\frac{-i\mu_B H_x + i\mu_B H_z}{2}$	0	$\frac{-i\mu_B H_y - i\mu_B H_z}{2}$	$\frac{\mu_B g_e (H_x + iH_y)}{2}$	$\frac{-\mu_B g_e H_z}{2}$	0	$\frac{i\mu_B H_x + i\mu_B H_y}{2}$
$\langle \alpha SP_3^3 \rvert$	$\frac{i\mu_B H_y - i\mu_B H_z}{2}$	0	$\frac{i\mu_B H_x + i\mu_B H_z}{2}$	0	$\frac{-i\mu_B H_x - i\mu_B H_y}{2}$	0	$\frac{\mu_B g_e H_z}{2}$	$\frac{\mu_B g_e (H_x - iH_y)}{2}$
$\langle \beta SP_3^3 \rvert$	0	$\frac{i\mu_B H_y - i\mu_B H_z}{2}$	0	$\frac{i\mu_B H_x + i\mu_B H_z}{2}$	0	$\frac{-i\mu_B H_x - i\mu_B H_y}{2}$	$\frac{\mu_B g_e (H_x + iH_y)}{2}$	$\frac{-\mu_B g_e H_z}{2}$

For our case the most important transition is the ground-state one ($g_0\mu_B H$). Therefore we use the matrix in the $|SP_0^3\alpha\rangle_1$, $|SP_0^3\beta\rangle_1$ basis as an example. The matrix was calculated knowing the operation of the angular momentum operators on the orbitals (P_x, P_y, or P_z) and spin α,β) functions.[24] The following 2×2 matrix is observed:

$$
\begin{array}{c|cc}
 & |SP_0^3\alpha\rangle_1 & |SP_0^3\beta\rangle_1 \\
{}_1\langle\alpha SP_0^3| & \left[\frac{g_e\mu_B H_z}{2}+\frac{\xi}{\Delta}\left[\frac{\mu_B H_z}{2}-\frac{\mu_B H_y}{4}-\frac{\mu_B H_x}{4}\right]\right] & \left[\frac{g_e\mu_B H_x}{2}-\frac{ig_e\mu_B H_y}{2}-\frac{\xi}{\Delta}\left[\frac{\mu_B H_z}{4}+\frac{\mu_B H_y}{4}-\frac{\mu_B H_x}{2}\right]-\frac{i\xi}{\Delta}\left[\frac{\mu_B H_y}{2}-\frac{\mu_B H_z}{4}-\frac{\mu_B H_x}{4}\right]\right] \\
{}_1\langle\beta SP_0^3| & \left[\frac{g_e\mu_B H_x}{2}+\frac{ig_e\mu_B H_y}{2}-\frac{\xi}{\Delta}\left[\frac{\mu_B H_z}{4}+\frac{\mu_B H_y}{4}-\frac{\mu_B H_x}{2}\right]+\frac{i\xi}{\Delta}\left[\frac{\mu_B H_y}{2}-\frac{\mu_B H_z}{4}-\frac{\mu_B H_x}{4}\right]\right] & \left[\frac{-g_e\mu_B H_z}{2}-\frac{\xi}{\Delta}\left[\frac{\mu_B H_z}{2}-\frac{\mu_B H_y}{4}-\frac{\mu_B H_x}{4}\right]\right]
\end{array}
.
$$

The diagonalization of a 2×2 Hermitian matrix is a textbook problem which leads to analytic expression for the eigenvalues and the eigenvectors. See Table I.

TABLE I. The energies in this table were calculated by diagonalization of four 2×2 matrices which were calculated as described in the text. In the left column the magnetic field is parallel to the Z direction, and in the right column, the field is parallel to the direction of the $|SP_0^3\rangle$ orbital, namely $H_x=H_y=H_z=H/\sqrt{3}$.

$E_1=\Delta+\frac{\mu_B H_z}{2}\left[2.002+2.002\frac{\xi}{\Delta}\right]$	$E_1=\Delta+\frac{\mu_B H}{2}(2.002)$
$E_2=\Delta-\frac{\mu_B H_z}{2}\left[2.002+2.002\frac{\xi}{\Delta}\right]$	$E_2=\Delta-\frac{\mu_B H}{2}(2.002)$
$E_3=-2.732\frac{\xi}{4}+\frac{\mu_B H_z}{2}\left[0.274+0.111\frac{\xi}{\Delta}\right]$	$E_3=-2.732\frac{\xi}{4}+\frac{\mu_B H}{2}\left[0.421+0.021\frac{\xi}{\Delta}\right]$
$E_4=-2.732\frac{\xi}{4}-\frac{\mu_B H_z}{2}\left[0.274+0.111\frac{\xi}{\Delta}\right]$	$E_4=-2.732\frac{\xi}{4}-\frac{\mu_B H}{2}\left[0.421+0.021\frac{\xi}{\Delta}\right]$
$E_5=0.732\frac{\xi}{4}+\frac{\mu_B H_z}{2}\left[1.976-0.456\frac{\xi}{\Delta}\right]$	$E_5=0.732\frac{\xi}{4}+\frac{\mu_B H}{2}\left[1.57-0.028\frac{\xi}{\Delta}\right]$
$E_6=0.732\frac{\xi}{4}-\frac{\mu_B H_z}{2}\left[1.976-0.456\frac{\xi}{\Delta}\right]$	$E_6=0.732\frac{\xi}{4}-\frac{\mu_B H}{2}\left[1.57-0.028\frac{\xi}{\Delta}\right]$
$E_7=2\frac{\xi}{4}+\frac{\mu_B H_z}{2}(2.218)$	$E_7=2\frac{\xi}{4}+\frac{\mu_B H}{2}(3.619)$
$E_8=2\frac{\xi}{4}-\frac{\mu_B H_z}{2}(2.218)$	$E_8=2\frac{\xi}{4}-\frac{\mu_B H}{2}(3.619)$

[1]G. Binnig, H. Rohrer, Ch. Gerber, and E. Weibel, Phys. Rev. Lett. **49**, 57 (1982).
[2]G. Binnig, H. Rohrer, Ch. Gerber, and E. Weibel, Phys. Rev. Lett. **50**, 120 (1983).
[3]V. M. Hallmark, S. Chiang, J. F. Rabolt, and J. D. Swalen, and R. J. Wilson, Phys. Rev. Lett. **59**, 2879 (1987).
[4]M. D. Pashley, K. W. Haberen, W. Friday, J. M. Woodal, and P. D. Kirchner, Phys. Rev. Lett. **60**, 2176 (1988).
[5]R. S. Becker, J. A. Golovchenko, E. G. McRae, and B. S. Swartzentruber, Phys. Rev. Lett. **55**, 2028 (1985).
[6]H. Ohtani, R. J. Wilson, S. Chiang, and C. M. Mate, Phys. Rev. Lett. **60**, 2398 (1988).
[7]Ph. Avouris and R. Wolkow, Phys. Rev. Lett. **60**, 1049 (1988).
[8]U. K. Köhler, J. E. Demuth, and R. J. Hamers, Phys. Rev. Lett. **60**, 2499 (1988).
[9]H. Tokumoto, K. Miki, Y. Morita, T. Sato, M. Iwatsuki, T. Fukuda, and M. Suzuki (unpublished).
[10]C. F. Quate, Phys. Today **39** (8), 26 (1986).
[11]S. Schneider, R. Sonnenfeld, P. K. Hansma, and J. Tersoff, Phys. Rev. B **34** 4979 (1986).
[12]D. M. Eigler and E. K. Schweizer, Nature, **344**, 524 (1990).
[13]J. K. Gimzewski, B. Reihl, J. H. Coombs, and R. R. Schlitter, J. Phys. B **72**, 497 (1988).
[14]P. Muralt and D. Pohl, Appl. Phys. Lett. **48**, 514 (1986).
[15]P. K. Hansma, B. Drake, O. Marti, J. A. C Gould, and C. B. Prater, Science **243**, 641 (1989).
[16]G. Binnig, C. F. Quate, and Ch. Gerber, Phys. Rev. Lett. **56**, 930 (1986).
[17]Y. Martin, D. W. Abraham, and H. K. Wickramasinghe Appl. Phys. Lett. **52**, 1103 (1988).
[18]J. M. R. Weaver, L. M. Walpita, and H. K. Wickramasinghe, **342**, 783 (1989).
[19]Y. Manassen, R. J. Hamers, J. E. Demuth, and A. J. Castellano, Jr., Phys. Rev. Lett. **62**, 2531 (1989).
[20]A. W. McKinnon and M. E. Welland (unpublished).
[21]Y. Nishi, Jpn. J. Appl. Phys. **10**, 52 (1971).
[22]P. J. Kaplan, E. H. Poindexter, B. E. Deal, and R. R. Razouk, J. Appl. Phys. **50**, 5847 (1979).
[23]K. L. Brower, Appl. Phys. Lett. **43**, 1111 (1983).
[24]A. M. Atherton, *Electron Spin Resonance, Theory and Applications* (Wiley, New York, 1973).
[25]W. Rohrbeck, E. Chila, H. Fröhlich, and J. Reidel, Appl. Phys. A **52**, 344 (1991).
[26]H. Rohrer, in *Scanning Tunneling Microscopy and Related Methods,* edited by R. J. Behm *et al.* (Kluwer Academic, Amsterdam, 1990).
[27]D. Shachal and Y Manassen, Phys. Rev. B **44**, 11 528 (1991).
[28]J. Kirtley, D. J. Scalapino, and P. K. Hansma, *ibid.* **14**, 3177 (1976).
[29]S. de Cheveigné, J. Klein, A. Léger, M. Belin, and D. Défourneau, Phys. Rev. B **15**, 750 (1977).
[30]A. Adane, A. Fauconnet, J. Klein, A. Léger, M. Belin, and D. Défourneau, Solid State Commun. **16**, 1071 (1975).
[31]J. K. Gimzewski, B. Reihl, J. H. Coombs, and R. R. Schlitter, J. Phys. B **72**, 497 (1988).
[32]S. de Cheveigné, J. Klein, and A. Léger, in *Tunneling Spectroscopy,* edited by Paul K. Hansma (Plenum, New York, 1982).
[33]B. N. J. Persson and J. E. Demuth, Solid State Commun. **57**, 769 (1986).
[34]S. N. Moltokov, Surf. Sci. **264**, 235 (1992).